JOURNAL OF MATERIALS SCIENCE 15 (1980) 2897–2914

Neck profiles in drawn linear polyethylene

P. D. COATES*, I. M. WARD
Department of Physics, University of Leeds, Leeds, UK

Neck profiles, neck propagation velocities and draw loads were measured for a series of linear polyethylene samples drawn in a tensile testing machine at 21, 75 and 100° C. The results were used to determine the profiles of strain, strain rate and draw stress in the neck. Elementary considerations show that the strain rate field in the neck relates to the strain hardening and to the strain rate sensitivity. A point of particular interest is that strain hardening appears to relate primarily to the polymer molecular weight whereas the strain rate sensitivity is more sensitive to the initial thermal treatment. The relationship of the present work to studies of true stress–true strain–true strain rate surfaces is discussed.

1. Introduction

The formation of a neck when polymers are stretched under appropriate conditions of strain rate and temperature has been the subject of considerable interest [1–6]. In some cases the neck stabilizes and continuous stretching can occur. The polymer is then reduced from its initial cross-section to its final cross-section in the process commonly termed cold drawing. Recent studies have shown that it is possible to cold draw linear polyethylene [7, 8] and other polymers [9, 10, 11] under conditions which yield very high draw ratios and very highly aligned structures with values of Young's modulus close to that anticipated on theoretical grounds. Studies of the necking behaviour of such polymers are therefore clearly of considerable practical value, since an understanding of this behaviour could provide a means of assessing polymers for various tensile deformation processes and give information on optimum processing conditions.

The present work attempts to relate the neck geometry and neck propagation to the true stress–strain–strain rate behaviour for a range of linear polyethylenes (LPE). These materials have previously been observed to exhibit widely differing neck geometries in tensile drawing, apparently depending upon such factors as molecular weight and the initial specimen morphology [12]. In this investigation we have attempted to obtain a more detailed understanding of these differences.

2. Experimental

2.1. Materials

In the recent investigations in our laboratory referred to above, the influence of molecular weight and initial thermal treatment on the drawing behaviour of linear polyethylene have been examined in considerable detail [7, 8, 12]. With regard to thermal treatment it was found that the initial morphology was primarily sensitive to the degree of supercooling. Extreme morphologies could be most conveniently produced either by direct quenching from the melt or by slow cooling at 5 to 10° C min^{-1}. Very extensive characterization of these initial morphologies for samples of widely different molecular weight characteristics have been described in several previous publications [8, 12, 13]. To establish continuity with this previous work and to enable the work described here to form a rational part of continuing investigations we have therefore followed what are now standard procedures in our laboratories for preparing samples of known morphology. The evidence of the previous work also enables us to be selective in our choice of starting materials. Polymer at three levels of molecular weight was chosen, the low molecular weight Rigidex® R50 grade, an

*Present address: School of Manufacturing Systems Engineering, University of Bradford, Bradford, UK.

0022–2461/80/112897–18$03.80/0

TABLE I LPE materials investigated

LPE Grade	Thermal history	$\bar{M}_w$	$\bar{M}_n$	Symbol
Hostalen GUR*	W†	$3.5–4 \times 10^6$	–	HGURW
H020 54P‡	S§	312 000	33 000	H020S
H020 54P‡	W	–	–	H020W
Rigidex 50‡	S	101 450	6 180	R50S
Rigidex 50‡	W	101 450	6 180	R50W

*Farbwerke Hoechst AG production grade.
†W is water quenched.
‡Production grades supplied by BP International Ltd.
§S is slow cooled.

intermediate molecular weight grade (HO20) and the ultra high molecular weight Hostalen (H) GUR (see Table I). To vary the morphology of the starting materials, the polymer granules or powder were compression moulded into sheets of thickness ~ 1 mm, at ~ 160° C, and then either quenched into water at ambient temperature, or allowed to cool slowly at ~ 8° C min^{-1} to room temperature. In the case of R50, quenching directly into the water from 160° C leads to a better defined spherulitic morphology than slow cooling does [8, 12, 13]. Similar results are obtained with the H020 grade, although the effects are less marked. Previous work suggested that the morphology of HGUR is little affected by thermal treatment, so for this polymer only water quenched specimens were investigated.

2.2. Neck profile measurements

There are certain variables in a tensile test which are chosen by the experimenter, the independent variables and other variables which are dependent. The independent variables include the material, specimen geometry, draw temperature, extension rate and draw time. The dependent variables include the draw load and neck profile geometry, from which the draw stress, strain and strain rate at points in the specimen can be calculated.

2.2.1. Independent variables

The "material variables" are summarized in Table I. A dumb-bell specimen geometry with gauge dimensions ~ 17 mm x ~ 4.7 mm was used, the specimens being cut from ~ 1 mm thick compression moulded sheets which were prepared in the manner described in Section 2.1. Cylindrical specimens would be most ideal for this investigation from the viewpoint of distribution of stress, but it is extremely difficult to produce cylindrical specimens which are of large enough diameter to allow accurate measurement of the neck profile. Slow cooling is necessary for the production of larger diameter rods, consequently their morphology cannot be varied.

The samples were drawn on an Instron tensile testing machine in an environmental chamber adapted for photographing the specimen whilst drawing proceeded. Three drawing temperatures (T), 100, 75 and ambient (~ 21° C), were investigated for each material. All specimens were allowed to reach thermal equilibrium at the higher temperatures before drawing. An extension rate (v_c) of 10 mm min^{-1} was employed in all tests. Although it is clearly possible to compare the results from different tests at various times, a drawing time suitably removed from the period of initial neck formation, $t = 200$ sec, was chosen for comparison of all specimens. Photographs of the drawing specimen were taken at fixed times (t), and drawing was terminated at $t = 300$ sec for all specimens. Drawing at a constant elongation rate, v, for a fixed time $t = t_d$ implies that a fixed value of "machine draw ratio", λ_m is imposed

$$\lambda_m = \frac{(v \times t_d) + \text{gauge length}}{\text{gauge length}} \quad (1)$$

Here, $\lambda_m \simeq 3$ at $t_d = 200$ sec.

2.2.2. Dependent variables

The dependent variables measured were the draw load, L, read from the load–time curve at $t =$ 200 sec, the neck profile and the neck propagation velocity, v_p. The neck profile measurement involved determination of the specimen width, $y(x)$ and thickness $z(x)$ as a function of axial distance, x, along the specimen (Fig. 1). Measurement of $y(x)$ was achieved photographically, so allowing determination of the neck profile in the width direction whilst drawing proceeded. Attempts were made to measure the neck profile

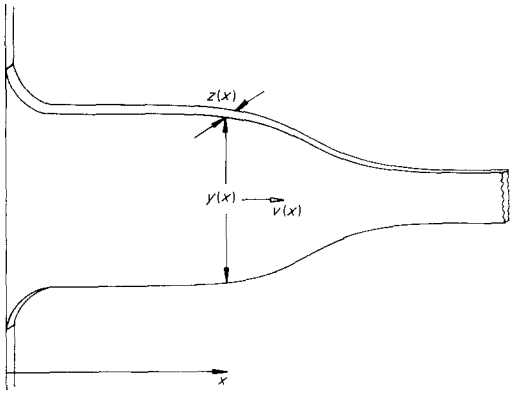

Figure 1 Neck co-ordinate system.

in the thickness direction simultaneously. A mirror mounted at 45° to the specimen enabled both the width and thickness of the drawing specimen to be photographed together. However, the accuracy of measurement of $z(x)$ proved to be too limited. Instead, the thickness $z(x)$ was measured by a travelling microscope for specimens removed from the tensile testing machine after being drawn for 300 sec. The width $y(x)$ of these specimens was also measured in the same manner for correlation of $y(x)$ and $z(x)$. These latter measurements clearly do not include any elastic component of deformation (unlike the measurements obtained photographically).

The draw ratio $\lambda(x)$ at any point along the specimen gauge length at time t is defined as

$$\lambda(x) = \frac{A_0}{A(x)} = \frac{y_0 z_0}{y(x)z(x)} \tag{2}$$

where A_0 is the original cross-sectional area (original width y_0, original thickness z_0) and $A(x)$ the cross sectional area at position x, at time t. Width and thickness measurements for specimens removed from the tensile testing machine showed that a linear relationship existed between $z(x)$ and $y(x)$, for $\lambda > 2$ for HGUR, H020 and R50W and for all λ for R50S, i.e.

$$z(x) \propto y(x)$$

or

$$\frac{z_0}{z(x)} = c\left(\frac{y_0}{y(x)}\right) \tag{3}$$

so that

$$\lambda(x) = c\left(\frac{y_0}{y(x)}\right)^2. \tag{4}$$

In passing, it is noted that for ideal cylindrical specimens the value of c should be unity. Values of c obtained from the measurement of $z(x)$ and $y(x)$ are given in Table II. Although these values are not unity, X-ray diffraction patterns of comparable samples show these to possess fibre symmetry, confirming that the deformation process is predominantly tensile.

TABLE II Values for $c = (Z_0/Z(x))(Y_0/Y(x))$, t = 300 sec

Material	c at 100° C	c at 75° C	c at ~ 21° C
HGUR W*	0.77	0.80	0.93
H020 W	0.71	0.74	0.81
H020 S†	0.55	0.60	0.77
R50 W	0.81	0.90	1.26
R50 S	1.0	1.0	–‡

*Water cooled.
†Slow cooled.
‡Brittle failure.

All specimens had gauge marks originally at 1 mm intervals along their length; changes in gauge mark separation give an alternative means of calculating $\lambda(x)$, thus allowing a check on the values of $\lambda(x)$ calculated from Equation 4 using values of c from Table II. (The gauge mark method for $\lambda(x)$ is not sufficiently accurate to be used alone in the neck region). In general, the results were in excellent agreement.

Further calculated quantities were the draw stress $\sigma(x)$ and the strain rate $\dot{\epsilon}(x)$ in the axial direction. The true draw stress $\sigma(x)$ was obtained from the relationship

$$\frac{L_t g}{A(x)} = \left(\frac{L_t g}{A_0}\right)\lambda(x) \tag{5}$$

where $g = 9.81\,\mathrm{m\,sec^{-2}}$ and L_t is the draw load at time t (t = 200 sec being chosen throughout the experiments), the other quantities also being related to time t. The true axial strain rate, $\dot{\epsilon}(x)$ at position x, time t, is found from

$$\dot{\epsilon}(x) = \frac{\mathrm{d}v(x)}{\mathrm{d}x} \tag{6}$$

where $v(x)$ is the axial velocity of material at x.

A general analysis of a neck will be complicated for two related reasons. First, the strain rate field may not be perfectly extensional. It would appear from our gridded specimens that the deformation is very close indeed to being extensional, and corresponds to the plug flow situation, similar to that assumed in our analysis of hydrostatic extrusion through a conical die [14]. Secondly, there will be a triaxial state of stress in the neck.

In the present paper all the other components of strain rate are considered negligible compared with the axial (elongational) strain rate. This assumption is justified for shallow necks i.e. necks exhibiting a gradual change in cross-section with axial distance. The work of Avitzur [15] on convergent flow shows that the only non-negligible component of strain rate is the radial strain rate, even at comparatively large angles to the axis of the convergent flow. The smaller the neck angle, the more accurately is the radial strain rate approximated by the axial strain rate. Also, the tensile elongational strain rate becomes extremely dominant in materials such as LPE, which exhibits a strong anisotropy of properties upon drawing. A discussion of the application of Avitzur's work to convergent plastic flow in polymers may be found in [14]. In general the necks observed in the present work are very shallow, the maximum angle included between the tangent to the neck at a point and the axial direction being of the order of 10°. In two extreme cases (R50W and H020W) the angle in a very small portion of the neck reached ~ 25°.

The variation of axial stress with position has been classically derived for approximately circular arc necks in metals, at the minimum section (see e.g. Hill [16]), which is not very applicable to the present work. Richmond and Devenpeck [17, 18] and Richmond and Morrison [19] have studied metal flow through sigmoidal dies, i.e. dies of very similar shape to the polymer necks studied here. They studied streamlined flow (when the velocity vector is everywhere coincident with a principal stress direction) based on the work of Shield [20] and generated stress equations applicable to the whole of the deformation zone, not just the minimum section. However their work relates to a rigid/perfectly plastic solid, which is not a good description of LPE. We have therefore been constrained to employ a simple mean axial stress, neglecting the variation of stress with perpendicular distance from the axis. This assumption is realistic, considering the shallowness of the necks and the first order effect of *axial* position on stress due to the developing anisotropy of the polymer, and is consistent with the assumption of plug flow.

2.3.3. Simple neck propagation model

Consider the neck profile for a fixed set of drawing conditions having a plane "isotropic boundary", AB shown in Fig. 2. As the neck propagates along the gauge length of the specimen the isotropic front moves along the specimen at some velocity $-v_p$. Alternatively, isotropic material is moving into the neck region (deformation zone) at a velocity v_p i.e. at a volumetric rate $v_p \cdot A_0$, where A_0 is the constant cross sectional area of isotropic material in the gauge length.

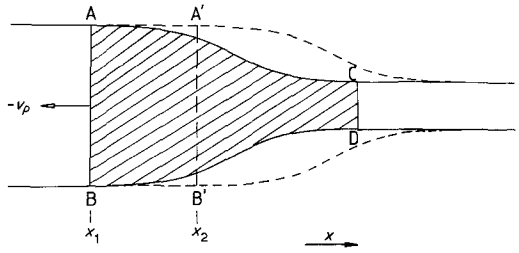

Figure 2 Simple neck propagation model.

Assuming conservation of volume in plastic deformation we have

$$A_0 \cdot v_p = A(x) \cdot v(x)$$

so that

$$v(x) = v_p \cdot \frac{A_0}{A(x)} = v_p \cdot \lambda(x) \qquad (7)$$

Therefore

$$\epsilon(x) = \frac{d[v_p \cdot \lambda(x)]}{dx}. \qquad (8)$$

The simplest modelling of isothermal neck propagation for given drawing conditions is to assume that the geometrical profile of the neck becomes constant after some initial formation period, and then moves along the gauge length at a constant velocity, v_p (Fig. 2). This leads to the expression for axial strain rate

$$\dot{\epsilon}(x) = v_p \frac{d\lambda(x)}{dx} \qquad (9)$$

i.e. $\dot{\epsilon}(x)$ is proportional to $d\lambda(x)/dx$ at any time when the neck is propagating (after initial neck formation), and $\dot{\epsilon}(x)$ can be obtained from $\lambda(x)$ values along the specimen. There is, of course, no reason why v_p should not vary for different materials, morphologies or drawing conditions. It is clear that measurement of v_p is necessary before the true axial strain rate can be calculated and the simple model checked. This measurement was achieved by means of the time-lapse photographs of each drawing specimen investigated. It was found, for a given specimen, that the neck profiles at different draw times could be superposed by a shift, Δx, in the x-direction, supporting the

TABLE III Neck profile velocities, v_p (mm sec^{-1})

Material	v_p at 100° C	v_p at 75° C	v_p at ~ 21° C
HGUR W*	~ 0.04†	~ 0.03†	~ 0.03†
H020 W	0.04	0.04	0.04
H020 S‡	0.03	0.03	0.01
R50 W	0.03	0.03	0.01
R50 S	~ 0.01§	0.02	–¶

*Water quenched.
†Almost homogeneous drawing makes determination of v_p very difficult.
‡Slow cooled.
§Neck profile not constant.
¶Brittle failure at $t \sim 0$ sec.

assumption of a fixed neck profile once the neck is propagating. The known time interval between photographs, together with Δx, then allowed the neck profile velocity to be calculated for each time interval. The limited results from this work suggests that the neck profile velocity, v_p, does remain constant whilst the neck is propagating (under the given experimental conditions). Values of v_p are given in Table III. One particular exception to the above observations was R50S at 100° C, where the neck profile did not remain constant. In this case the specimen showed evidence that the neck might not stabilize, i.e. thinning down occurred throughout the whole drawing experiment. With reference to Table III the applied extension rate was $v = 10\,\text{mm min}^{-1} = 0.167\,\text{mm sec}^{-1}$, i.e. considerably greater than the neck propagation velocities measured.

It was therefore possible to determine the true draw stress $\sigma(x)$, the draw ratio $\lambda(x)$ {and hence the true strain $\epsilon(x) = \ln[\lambda(x)]$} and the true axial strain rate $\dot{\epsilon}(x)$ simultaneously at any position x in the deformed material. It is again noted that the measurements include a component due to elastic deformation since they were determined from specimens in the course of being drawn.

In the simple steady state neck propagation model, isothermal conditions were assumed. We did not measure temperature profiles in the neck. However, our tests were conducted on relatively thin specimens at low extension rates. These factors, together with the developing axial thermal conductivity [21] through the neck should ensure that any adiabatic heating is minimal and can be neglected. Vincent [1] gives a rough estimation of the temperature gradient in a neck: using his figures for polyethylene a temperature gradient through the neck of around 5° C may be expected for specimens being drawn at room temperature. Recent work on thermal effects in necks [22] further suggests that for room temperature drawing of a linear polyethylene at 10 mm min^{-1} less than 10% of the mechanical work is converted into heat which increases the temperature of the specimen, the remainder being lost to the surroundings. It is clear that if there is a deviation from isothermal conditions then the propagation of the neck will be affected. Non-isothermal conditions are discussed briefly in Section 4.2.2.

3. Results

Since, under the experimental conditions described here, the neck appeared to attain a constant profile and propagate at a constant velocity (except in the case of R50S), a general comparison of results for different materials at a fixed drawing time (here $t = 200$ sec) can be made.

3.1. Geometrical neck profiles

In all cases the necks in geometric terms were shallow. H020W and R50W showed the sharpest necks, but even in these the maximum included angle encountered between a tangent to the neck and the axis was ~ 25°. In H020S and R50S the maximum angles were 10° and 15° respectively, and very shallow necks indeed were observed in HGRW, which appeared to draw almost homogeneously. Typical neck profiles for 100° C and $t = 200$ sec are shown in Fig. 3 to illustrate the contrast between the different materials.

3.2. Draw ratio profiles, $\lambda(x)$

Figs. 4a, b and c show the variation of draw ratio $\lambda(x)$ with axial distance along the specimen, at $t = 200$ sec and 100, 75 and 21° C respectively. The flatter the $\lambda(x)$ curve, the more homogeneous is the drawing. Conversely no flattening of the draw profile implies unstable drawing. Completely homogeneous drawing in the gauge length region would result in a draw ratio equal to the machine draw ratio, $\lambda_m = 2.96$ at $t = 200$ sec (assuming a gauge length of exactly 17 mm). As noted above (Section 3.2.) HGURW exhibits almost homogeneous drawing with $\lambda(x) = 3$ at most points along the gauge section at all three drawing temperatures. In general the remainder of the specimens exhibit a draw ratio profile which becomes flatter as the draw temperature is decreased, and the maximum draw ratio λ_{max}, falls with decreasing draw temperature.

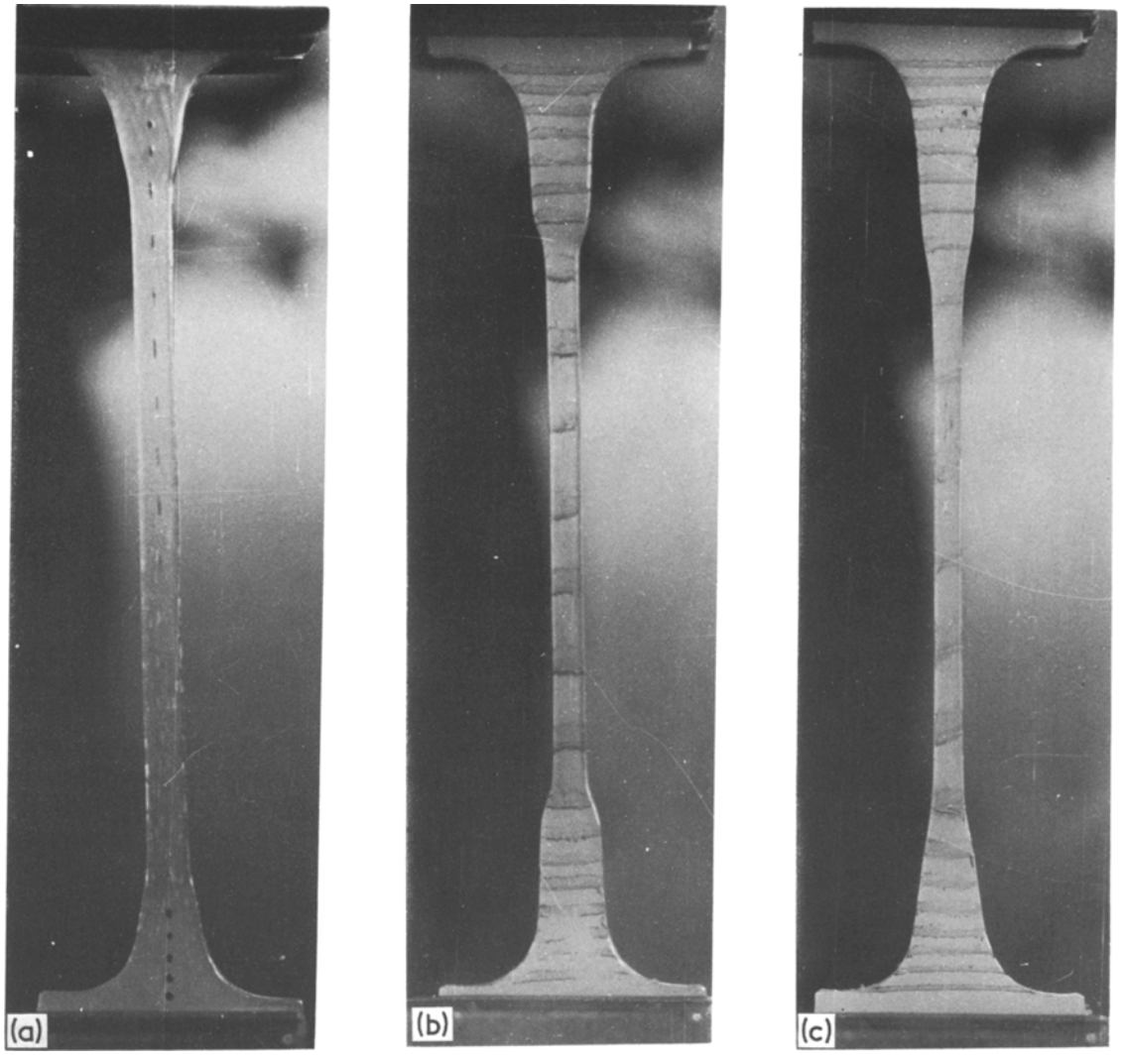

Figure 3 Neck profiles photographed whilst the specimens were being drawn, at $t = 200$ sec. Elongation rate = 10 mm min^{-1}. (a) HGUR, 100° C, (b) H020 W, 100° C, (c) H020 S, 100° C, (d) R50 W, 100° C, (e) R50 S, 100° C.

The region in which $\lambda(x)$ changes rapidly with distance x clearly corresponds to the section ABCD (Fig. 2) of the neck, and it is in this region of the neck that large changes in strain rate are expected (see Section 3.4.). Of practical interest in the draw ratio profile is the value of draw ratio produced through the neck (since the change in physical properties imparted by drawing is generally related to the draw ratio). For stabilized necks, the draw ratio produced through the neck is the value λ_{max} referred to above. The values of λ_{max} observed in the present work are collected in Table IV. It is quite apparent from these results that as the molecular weight $\bar{M}_w$ increases so the draw ratio produced through the neck decreases. Slow cooled morphologies appear to lead to higher values of draw ratio, and in general exhibit shallower necks. Drawing temperature appears to have little effect on the λ_{max} values for HGUR and H020, whereas λ_{max} decreases with temperature for R50 (except R50W at 21° C). R50S is again noted for its considerable difference in drawing behaviour: at 100° C the specimen appears to be thinning consistently along its length. At 75° C a steady λ_{max} has not been attained at $t = 200$ sec, but this is not due so much to unstable drawing as to the high value of λ_{max} for this material under the given drawing conditions [8].

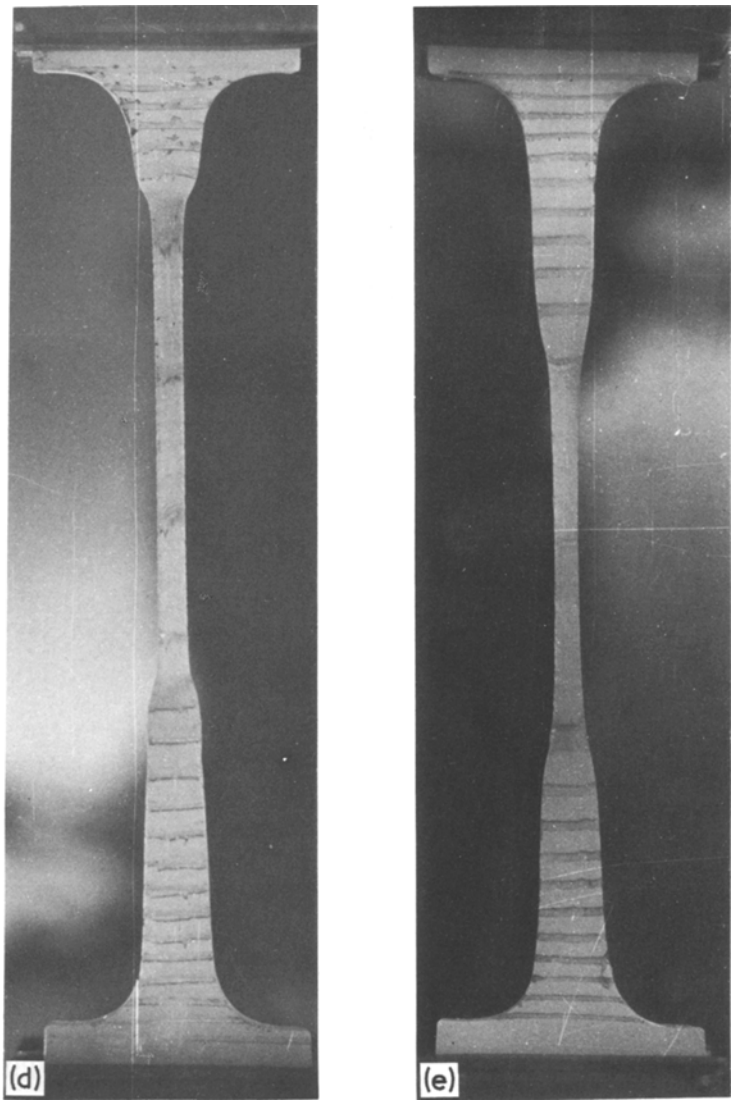

Figure 3 Continued.

3.3. Draw stress profiles

At an instant in the drawing process, all elements along the length of the specimen experience the same load, L, but have differing cross-sectional areas, $A(x)$, and hence draw ratios $\lambda(x)$. The draw stress and draw ratio are therefore linearly related, i.e.

$$\sigma(x) = \frac{Lg}{A(x)} = \frac{Lg\lambda(x)}{A_0} \qquad (10)$$

which is the Considère relationship. Fig. 5 shows the Considère lines for $t = 200$ sec. In all cases the slope of the Considère line increases as the drawing temperature falls.

Although simple trends due to morphology or molecular weight are not very evident, certain observations can be made. The lowest molecular weight polymer in its slow cooled morphology (R50S) exhibits the lowest slope at 100° C and the greatest change in slope with decreasing temperature, finally failing in a brittle manner at 21° C, presumably because the yield stress then exceeds the fracture stress. This behaviour is consistent with the conclusion that the effects of draw temperature will be greatest for low molecular weight polymers where the junction points of the molecular network involved in the drawing process include crystalline regions as well as physical entanglements, especially in slow-cooled morphologies [12]. The drawing behaviour is then

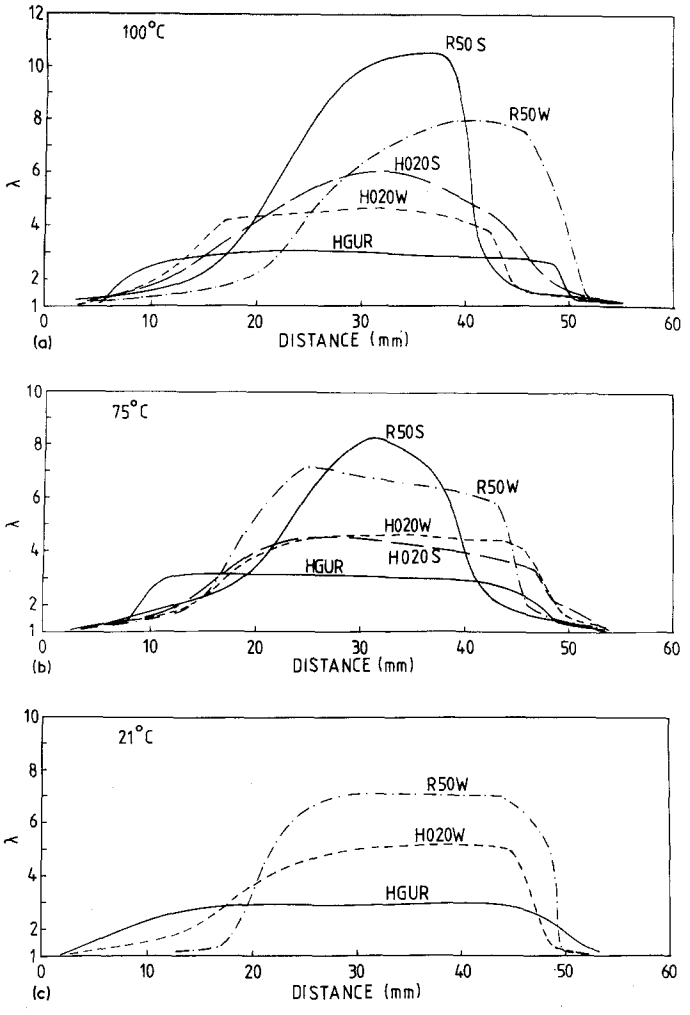

Figure 4 Draw ratio, λ versus axial distance (x) at $t = 200$ sec.

very sensitive to initial morphology. Furthermore we observe the greatest temperature sensitivity of drawing behaviour because the latter is now greatly influenced by the molecular mobility associated with the α-relaxation process.

The Considère lines in Fig. 5 relate to a specific drawing time. In general the drawing load, once having risen to the same maximum value at initial yield, then having fallen as neck formation became visible, remained at an approximately steady value as the neck propagated. The drawing load tended to rise slightly (especially at the lower temperatures), except for R50S at 100° C where the load fell continuously after the load maximum.

TABLE IV Values of draw ratio, λ_{max}, produced through the neck at $t = 200$ sec. λ_{max} measured by gauge mark separation

Material	λ_{max} at 100° C	λ_{max} at 75° C	λ_{max} at 21° C
HGUR W	3	3	3
H020 W	4.5	4.5	5
H020 S	5	5	5
R50 W	8	7	8.5
R50 S	~ 10	~ 9	–*

*Brittle failure.

3.4. Strain rate profiles

The true axial strain rate $\dot{\epsilon}(x)$ was calculated from Equation 8, using the values of v_p from Table III and calculated values of $d\lambda(x)/dx$. The latter values were obtained by determining the specimen width $y(x)$, then calculating the draw ratio $\lambda(x)$ as a function of x on the basis of change in cross-sectional area (see Section 2.2.2.). This method allows accurate measurement in the neck region where $\lambda(x)$ changes rapidly with x, which would not be possible using conventional gauge marks. (The gauge mark separation did, however, give a useful cross check on the values of $\lambda(x)$ calculated

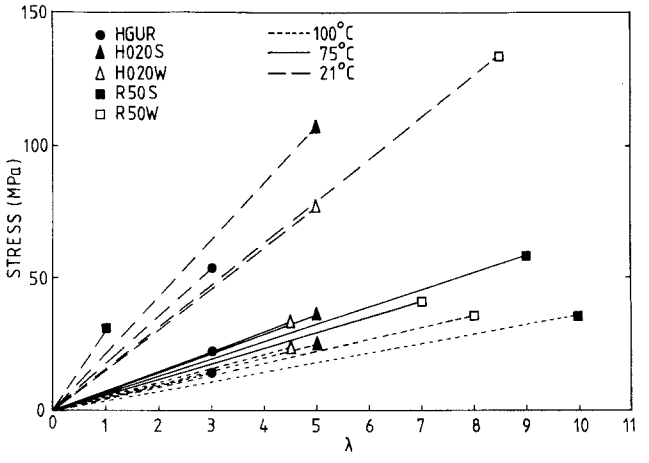

Figure 5 Considère lines for specimens being drawn, at $t = 200$ sec.

by the area method). It is perhaps worth noting here that the general dependence of v_p on polymer grade, morphology, drawing temperature, etc. prevents a meaningful comparison of results using draw ratio gradients, $d\lambda(x)/dx$ alone.

By way of example, computed values of $\dot{\epsilon}(x)$ are shown in Fig. 6 for a draw temperature of 100° C. Fig. 6 also includes a section of the draw ratio profile (by area measurement) for comparison. As expected there is a clear peak in strain rate in all cases, corresponding, of course to the region of highest draw ratio gradient. In general the geometrically sharper necks (H020W and R50W) have a narrower strain rate peak, but with higher maximum strain rate. For comparison, the initial "machine" strain rate was $\dot{\epsilon}_{m_i} = 9.8 \times 10^{-3}\ \text{sec}^{-1}$. Since the machine strain rate, $\dot{\epsilon}_m = v/l_t$ where v is a constant cross head speed and l_t the gauge length at time t, $\dot{\epsilon}_m$ decreases from $\dot{\epsilon}_{m_i}$ with increasing time. The machine strain rate at $t = 200$ sec is $\dot{\epsilon}_m = 3.3 \times 10^{-3}\ \text{sec}^{-1}$. The peak strain rates for H020W and R50W are therefore about two orders of magnitude greater than $\dot{\epsilon}_m$ at $t = 200$ sec.

It is more meaningful to consider the relationship between the strain rate $\dot{\epsilon}(x)$ and the draw

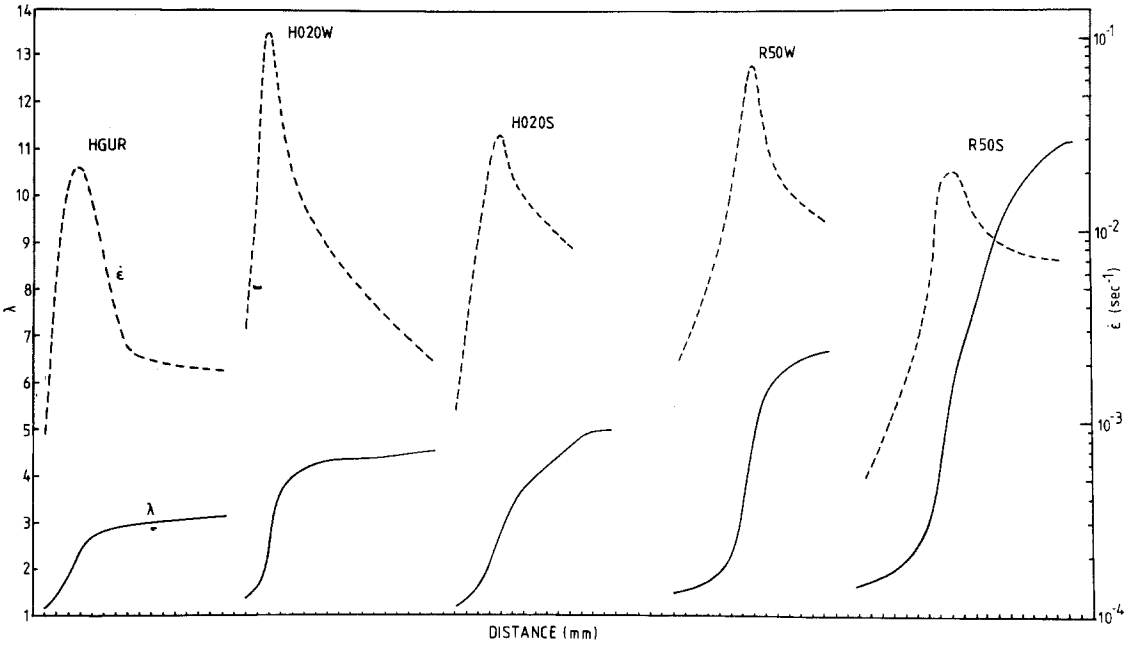

Figure 6 Variation of axial strain rate, $\dot{\epsilon}$ with axial distance (x) at $t = 200$ sec. Draw ratio profiles are included for comparison (up to λ_{max}).

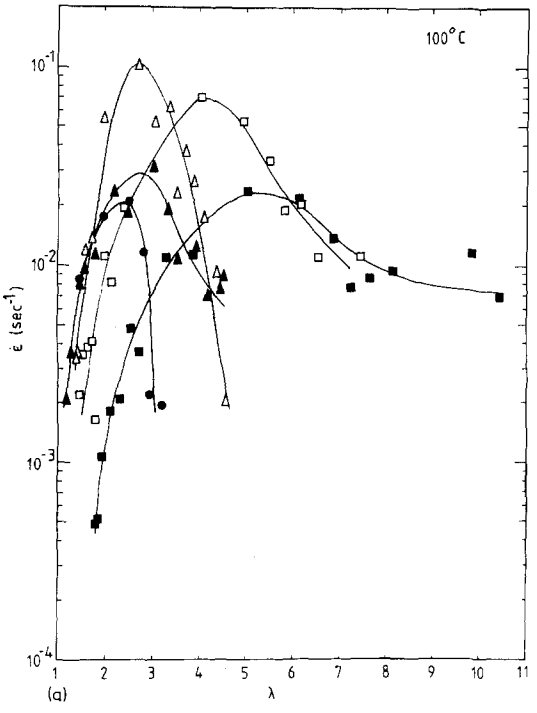

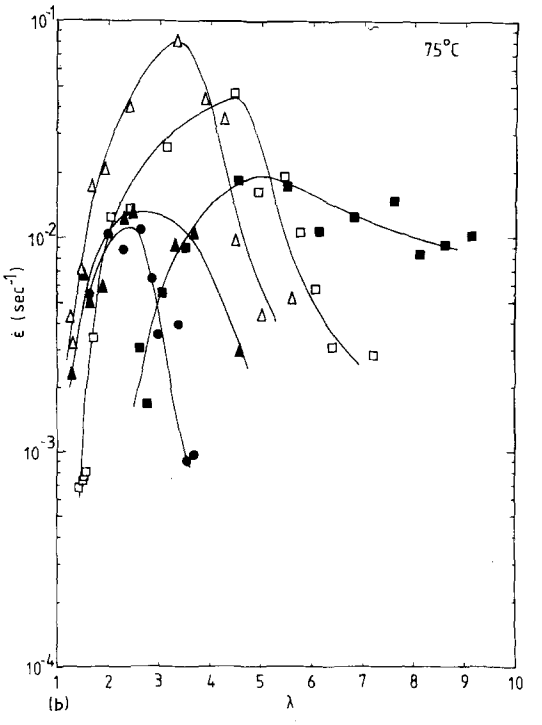

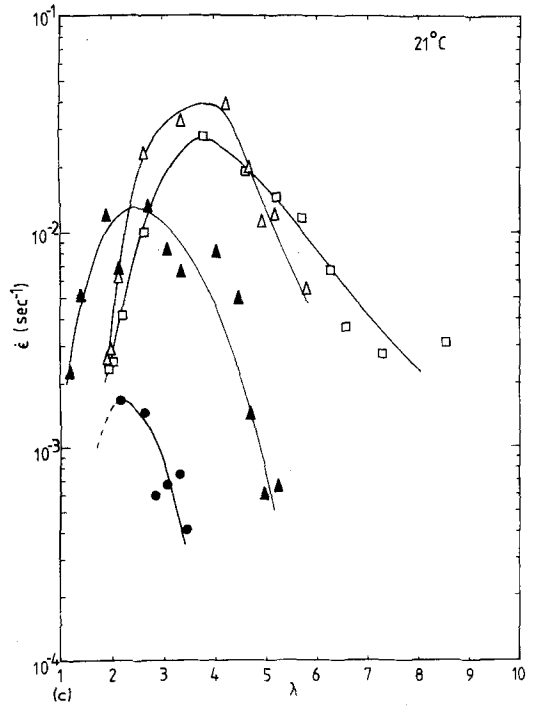

Figure 7 Variation of axial strain rate, $\dot{\epsilon}$ with draw ratio, λ at $t = 200$ sec. (● HGUR △ H020W ▲ H020S □ R50W ■ R50S), (a) 100° C (b) 75° C (c) 21° C.

ratio $\lambda(x)$, as shown in Figs. 7a, b and c for drawing temperatures of 100, 75 and 21° C respectively. At 100° C a molecular weight effect may be discerned, in that the curves can be categorized into three draw ratio regions according to the LPE grade tested: (1) Denoting the value of $\lambda(x)$ at which $\dot{\epsilon}(x)$ is a maximum by λ_{peak}, HGUR exhibits a strain rate peak at the lowest value of λ_{peak} (~ 2.4) observed for any of the specimens, and also exhibits the narrowest range of $\lambda(x)$ in the peak. (2) H020W and H020S show strain rate peaks at the same draw ratio ($\lambda_{peak} \sim 2.7$) and have a similar range of $\lambda(x)$ in the peak (but broader than for HGUR). (3) R50W and R50S exhibit $\dot{\epsilon}(x)$ peaks at higher draw ratios ($\lambda_{peak} = 4$ and 5 respectively) and also have the greatest range of draw ratio in the strain rate peak. A similar situation holds at 75 and 21° C, although the R50W and R50S peaks appear to be separating at 75° C; similarly H020S and H020W at 21° C. The essential shapes of the strain rate–draw ratio profiles do not change greatly with drawing temperature, nor does the value of λ_{peak} for each material. This reflects only slight changes, in general, of the geometrical neck profile for isothermal drawing.

Having observed molecular weight effects in the $\dot{\epsilon}(x)$–$\lambda(x)$ peaks, there also appears to be a tendency for morphology to affect the strain rate values observed. For both H020 and R50,

the value of $\dot{\epsilon}_{max}$ is considerably greater in the water quenched samples.

In previous studies of the effects of morphology and molecular weight on the drawing behaviour of LPE [12] attention was focused on the maximum draw ratio in the sample as a function of time of draw. In contrast to the situation for R50 where the different thermal treatments produced very different draw ratio/time plots, the latter were indistinguishable in the case of H020. The present results show that the neck shape is, however, still affected by initial thermal treatment in H020, although the effects are much less marked than in R50.

4. Discussion of factors which determine neck profiles

We shall now seek a fuller understanding of the neck profiles and neck propagation in terms of (i) the imposed boundary conditions and (ii) the deformation behaviour of the polymer.

4.1. Imposed boundary conditions

First, consider the simple model of the neck shown in Fig. 2, and discussed in Section 2.2.2. In this simple model it is assumed that deformation only occurs inside the deformation zone (shaded) at any instant, i.e. $\dot{\epsilon} = 0$ outside the deformation zone at that instant. There will be a particular strain rate field associated with the deformation zone, in which $\dot{\epsilon}$ may reach relatively high values at some points, and relatively low values at other points, as has been observed in Section 3.4. and this strain rate field is related to the geometrical neck profile through the draw ratio (Section 3.4.).

In the presence of a neck, the average axial strain rate can be obtained from consideration of one half of the specimen (Fig. 8) assuming symmetry of deformation. This was always the case, both necks propagating simultaneously. We have

$$\bar{\dot{\epsilon}}(x) = \frac{1}{(l_t/2)} \int_0^{l_t/2} \dot{\epsilon}(x)\, dx. \qquad (11)$$

For deformation at constant volume

$$\bar{\dot{\epsilon}}(x) = \frac{dv(x)}{dx} = v_p \frac{d\lambda(x)}{dx} \qquad (12)$$

and

$$\bar{\dot{\epsilon}}(x) = \frac{2v_p}{l_t} \int_{\lambda=1}^{\lambda_{max}} d\lambda = \frac{2v_p}{l_t}(\lambda_{max} - 1). \qquad (13)$$

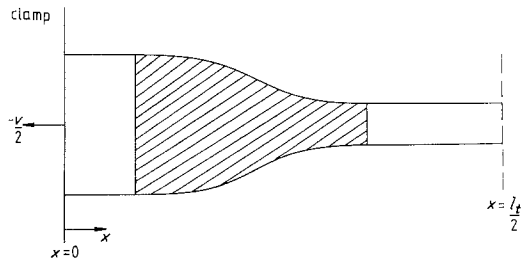

Figure 8 Values of variables for calculation of average axial strain rate.

Now for a given drawing temperature, there exists only one externally imposed constraint on the polymer in a tensile test, namely the fixed elongation rate v. This constraint requires the *average* axial strain rate $\bar{\dot{\epsilon}}(x)$, along the specimen gauge length, l_t to be equal to the machine strain rate $\dot{\epsilon}_m$, at a given instant in time i.e.

$$\bar{\dot{\epsilon}}(x) = \dot{\epsilon}_m = \frac{v}{l_t} \qquad (14)$$

Combining Equations 13 and 14 we have

$$v_p = \frac{v}{2(\lambda_{max} - 1)}. \qquad (15)$$

The neck profile velocity v_p therefore depends on the externally imposed boundary conditions of a constant elongation rate, v, *and* on the draw ratio produced through the neck, λ_{max}, which in turn appears to be dependent on the molecular weight grade of LPE, and so is determined by the polymer.

Values of neck propagation velocity v_p calculated from Equation 15 using λ_{max} values from Table IV are given in Table V. The agreement is reasonable, considering the limited accuracy in measuring v_p. Homogeneous drawing would give a machine draw ratio $\lambda_m = 2.96$ at $t = 200$ sec, which sets a limiting value of v_p for any specimen which exhibits a neck, namely $v_p = v/[2(\lambda_m - 1)] = 0.048\,mm\,sec^{-1}$ in the present case.

4.2. Material deformation behaviour

The above discussion covered the externally imposed condition on the strain rate field (which is, of course, reflected in the geometrical neck profile). Equation 11 has to be obeyed whatever the material, morphology, drawing temperature, etc. However, subject to this condition the material properties determine the actual strain rate field,

TABLE V Calculated values of neck profile velocity v_p (mm sec^{-1}) at $t = 200$ sec. Measured values, are shown in parentheses

Material	v_p at 100° C	v_p at 75° C	v_p at 21° C
HGUR	0.04 (~ 0.04)	0.04 (~ 0.03)	0.04 (~ 0.03)
H020 W	0.024 (0.04)	0.024 (0.04)	0.021 (0.04)
H020 S	0.021 (0.03)	0.021 (0.03)	0.021 (0.01)
R50 W	0.012 (0.03)	0.014 (0.03)	0.011 (0.01)
R50 S	0.010 (0.01)	0.010 (0.02)	–

and hence the actual neck profile observed. Testing different materials under the same externally imposed conditions of extension rate and temperature will therefore allow observation of the effect of material properties.

We will now explore the possibility that for a given drawing temperature, and assuming isothermal conditions, the differences between the various neck profiles observed in the present work for different LPE grades can be related to differences in the relationships between the true stress, true strain and true strain rate for each grade.

The strain rate–draw ratio curves (Fig. 6) are particularly relevant here since, of all the measurements obtained from the neck, they reflect most directly the deformation behaviour of the polymer, taking into account the fact that the true stress is increasing linearly with draw ratio. (A plot of strain rate against true stress, would of course be equally meaningful and would have the same form as the $\dot{\epsilon}$–λ curves).

4.2.1. Strain hardening and strain rate sensitivity

Before considering the deformation behaviour of specific LPE grades, we shall discuss some aspects of deformation related to the neck profile: this will provide some insight into the observed forms of the $\dot{\epsilon}$–λ curves.

Consider an element of the specimen being drawn isothermally, the element being at some draw ratio λ, experiencing a stress σ and deforming at some strain rate $\dot{\epsilon}$, at time t.

For the purpose of clarity, the draw ratio, λ, will be used there – as elsewhere in the present work – as the measure of strain rather than the "true strain", $\epsilon = \ln \lambda$. The conventional definition of strain rate, $\dot{\epsilon} = d\epsilon/dt = (1/\lambda)(d\lambda/dt)$ will be retained. Substitution of true strain for draw ratio would, of course, not materially affect the following discussion.

The values of σ, λ and $\dot{\epsilon}$ will not be independent, since the polymer exhibits fixed true stress–strain, strain rate surfaces at fixed temperatures [4]. At time t the element under consideration can be represented by some point, A, on the true σ–ϵ–$\dot{\epsilon}$ surface for temperature T. Let there then be an increase $d\lambda$, in the draw ratio of the element (in time dt). The element will now be "mapped" at a different point, B, $(\sigma + d\sigma, \dot{\epsilon} + d\dot{\epsilon})$ on the true σ–λ–$\dot{\epsilon}$ surface. The total change in stress, $d\sigma$ due to this change $d\lambda$ may be expressed using the total differential form

$$d\sigma = \left(\frac{\partial \sigma}{\partial \lambda}\right)_{\dot{\epsilon}} d\lambda + \left(\frac{\partial \sigma}{\partial \dot{\epsilon}}\right)_{\lambda} d\dot{\epsilon}. \qquad (16)$$

Equation 16 shows that the total change in stress has components due to the change in λ and any change in $\dot{\epsilon}$ incurred. From the Considère relationship, fixing the increase $d\lambda$ automatically fixes the change in stress $d\sigma$ (for a constant draw force): $d\sigma = (F/A_0)d\lambda$. It is therefore of interest to consider any changes in strain rate. Fig. 9 shows the situation in terms of the σ–λ plane for the cases where the Considere line lies (a) above and (b) below the σ versus λ curve for constant strain rate, $\dot{\epsilon}$ (σ, λ and $\dot{\epsilon}$ referring to the state of the element at A).

If, as in Fig. 9a, $d\sigma > (\partial\sigma/\partial\lambda)_{\dot{\epsilon}}\, d\lambda$ then, from Equation 16

$$\left(\frac{\partial \sigma}{\partial \dot{\epsilon}}\right)_{\lambda} d\dot{\epsilon} > 0$$

i.e. $d\dot{\epsilon} > 0$ (since the slope of stress–strain rate plots at a constant draw ratio has always been observed to be positive (e.g. [4, 23]). Therefore, an increase in λ and σ clearly leads to an increase in strain rate in this case, and the element is described by point B in Fig. 9a.

If, however, the situation of Fig. 9b pertains, i.e. $d\sigma < (\partial\sigma/\partial\lambda)_{\dot{\epsilon}}\, d\lambda$ then from Equation 16 $(\partial\sigma/\partial\dot{\epsilon})_{\lambda}\, d\dot{\epsilon} < 0$ i.e. $d\dot{\epsilon} < 0$, and in this case the increase in λ and σ lead to a decrease in strain rate. The element is then described by point B′ in Fig. 9b.

The former case, that of increasing σ and λ

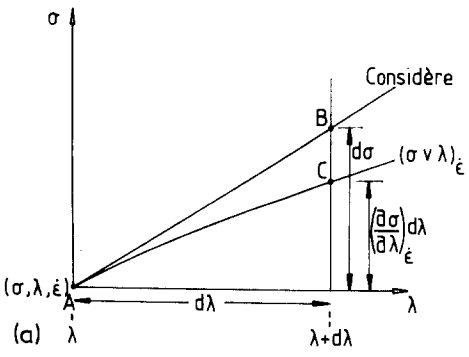

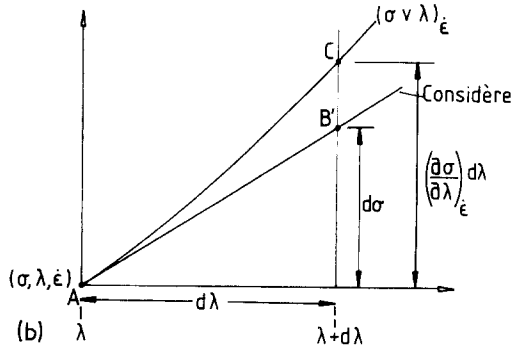

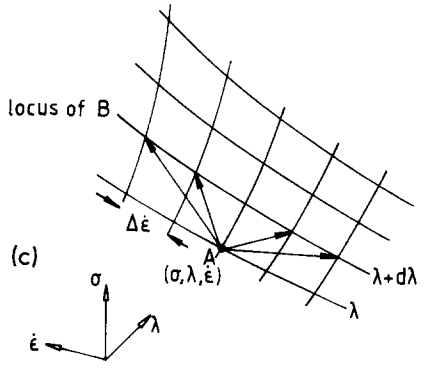

Figure 9 Consideration of path followed by an element during deformation: in the stress (σ) – draw ratio (λ) plane for the cases where the Considère line lies (a) above and (b) below the σ–v–λ curve for the value of strain rate, $\dot{\epsilon}$ pertaining to point A; (c) some possible paths across the σ–v–$\dot{\epsilon}$ surface for a specific increment, $d\lambda$, in draw ratio.

leading to an increase in $\dot{\epsilon}$ has been observed in the initial (low λ) parts of the neck (see Fig. 7). The latter case, in which $\dot{\epsilon}$ decreases as σ and λ increase was observed for the higher draw ratio parts of the neck (Fig. 7).

Fig. 9c illustrates some possible paths across the true σ–λ–$\dot{\epsilon}$ surface which could describe the deformation of the element. The contour ($\lambda + d\lambda$) represents the locus for the point B, representing the state of the element after a draw ratio increase $d\lambda$, but the specific location of B depends on the actual value of the total change in strain rate, $d\dot{\epsilon}$.

Consider now the λ–$\dot{\epsilon}$ plane: the total change in strain rate incurred by an increase in λ of $d\lambda$ can be expressed, using Equation 16, as

$$d\dot{\epsilon} = \frac{d\sigma - \left(\frac{\partial\sigma}{\partial\lambda}\right)_{\dot{\epsilon}} d\lambda}{\left(\frac{\partial\sigma}{\partial\dot{\epsilon}}\right)_{\lambda}} \qquad (17)$$

or

$$\frac{d\dot{\epsilon}}{d\lambda} = \frac{\frac{d\sigma}{d\lambda} - \left(\frac{\partial\sigma}{\partial\lambda}\right)_{\dot{\epsilon}}}{\left(\frac{\partial\sigma}{\partial\dot{\epsilon}}\right)_{\lambda}}. \qquad (18)$$

$d\dot{\epsilon}/d\lambda$ represents the specific direction of the path across the true σ–λ–$\dot{\epsilon}$ surface (see Fig. 10).

In the first case (path AB_1), $(d\sigma/d\lambda) > (\partial\sigma/\partial\lambda)_{\dot{\epsilon}}$ so that $d\dot{\epsilon} > 0$ and the path lies at a positive angle θ where $\theta = \tan^{-1}(d\dot{\epsilon}/d\lambda)_{\sigma}$.

In the second case, path AB_2, $(d\sigma/d\lambda) < (\partial\sigma/\partial\lambda)_{\dot{\epsilon}}$ so that $d\dot{\epsilon} < 0$ and the path lies at a negative angle α where $\alpha = \tan^{-1}(-d\dot{\epsilon}/d\lambda)_{\sigma}$. The actual magnitude of the change in strain rate for a fixed change in λ depends on the relative magnitudes of the numerator and denominator in Equation 18. The numerator includes a conventional strain hardening term $(\partial\sigma/\partial\lambda)_{\dot{\epsilon}}$ and the denominator is related to the strain rate sensitivity of the material,

$$\left(\frac{\partial\sigma}{\partial \ln\dot{\epsilon}}\right)_{\lambda} = \frac{1}{\dot{\epsilon}}\left(\frac{\partial\sigma}{\partial\dot{\epsilon}}\right)_{\lambda}.$$

Two extreme cases may now be identified. There will be a very large positive change in strain rate in the element if both the strain hardening is small compared to $d\sigma/d\lambda$ and the strain rate sensitivity is low. Conversely, there will be a very large negative change in strain rate in the element if the strain hardening is very great compared to $d\sigma/d\lambda$ and the strain rate sensitivity of the material is again low.

If the neck is assumed to propagate at constant draw load and speed, with a fixed profile, then by implication each element of material will follow the same path across the true σ–λ–$\dot{\epsilon}$ surface. In accordance with the above discussion, this path will be fixed by the strain hardening behaviour and strain rate sensitivity of the polymer (these being, in effect the slopes of the σ–λ–$\dot{\epsilon}$ surface) subject to the overall constraint imposed by the

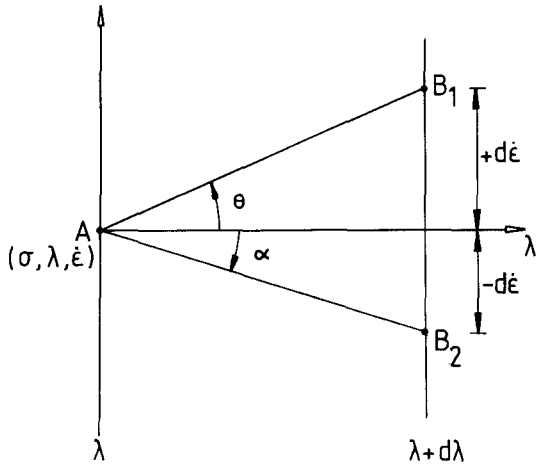

Figure 10 Draw ratio (λ) – strain rate ($\dot{\epsilon}$) section of the true σ–λ–$\dot{\epsilon}$ surface: change in strain rate for a specific increment, $d\lambda$, in λ.

average strain rate. The differences in neck profile are therefore expected to depend on differences in the strain hardening behaviour and strain rate sensitivity of the different materials tested. These parameters depend on σ, λ, $\dot{\epsilon}$, temperature and pressure etc. to differing degrees for each material; this will be reflected in such factors as the geometrical sharpness of the neck and the draw ratio produced through the neck in different materials. For example, a material exhibiting a very high degree of strain hardening even at low draw ratios and also having a very high strain rate sensitivity (i.e. a large change in stress is required to produce a small change in strain rate) will draw in a fairly homogeneous manner, with only small evidence of necking, and the draw ratio produced through the neck will be low. Such appears to be the case for the ultra high molecular weight sample, HGUR. The other extreme case is a material exhibiting a very low degree of strain hardening at all draw ratios, and also having a very low strain rate sensitivity. This material is highly likely to neck sharply to high draw ratios, and fail in tensile drawing, i.e. the neck will not be stabilized. The intermediate cases are numerous depending on the combination of strain hardening and strain rate sensitivity and how these quantities change with λ, σ and $\dot{\epsilon}$. A low strain rate sensitivity will lead to a high strain rate peak in the neck. Conversely, a higher strain rate sensitivity will lead to a lower strain rate peak in the neck. A high strain hardening behaviour at all draw ratios will lead to a low draw ratio through the neck, whereas low strain hardening at low λ but which increases with λ may allow a high draw ratio to be produced through the neck. At low λ a higher strain hardening behaviour will tend to shift the value of λ_{peak}, which corresponds to the peak strain rate, $\dot{\epsilon}_{peak}$ to lower values, and will tend to narrow the $\dot{\epsilon}$–λ peak.

Table VI provides a qualitative summary of the effects of some of the combinations of strain hardening and strain rate sensitivity at low draw ratios. Considering Fig. 7a in the light of the above discussion, several inferences are possible. It appears that at 100° C HGUR possesses both a high strain hardening behaviour and a high strain rate sensitivity at low draw ratios, as discussed above. H020 appears to possess a lower strain hardening behaviour than HGUR but higher than R50. Also, the slow cooled H020S exhibits a higher strain rate sensitivity than the water quenched H020W. R50 exhibits the lower strain hardening behaviour, and again the slow cooled sample has a greater strain rate sensitivity than the water quenched sample. A similar order holds for the lower drawing temperatures, 75 and 21° C (Figs. 7b and c). It may therefore be inferred that the morphology of the R50 and H020 grades strongly influences the strain rate sensitivity, whereas the molecular weight strongly influences the strain hardening behaviour. It is interesting to note that HGUR shows the highest strain rate sensitivity of all the materials examined. In this polymer the deformation behaviour is associated with the molecular network, and effects of morphology would not be expected to be significant. These factors suggest a possible "screening" of grades of LPE for predominantly tensile deformation processes, and give an indication of the limitations of different grades.

It was noted in Section 4.4 that the value of λ_{peak} corresponding to $\dot{\epsilon}_{peak}$ for each material did not change greatly with (isothermal) drawing temperature. The draw ratio produced through the neck, λ_{max} (Table IV) also did not change greatly with draw temperature. This suggests that the strain hardening behaviour of each material changes in a uniform manner at all draw ratios up to λ_{max} with variation in the drawing temperature, in the range investigated. The change in $\dot{\epsilon}_{peak}$ values with draw temperature is also not very marked, so that the overall effect is to maintain a similar neck profile with change in set draw temperature.

The approximate steady value of draw load which was observed during neck propagation will

TABLE VI Qualitative effects of strain rate sensitivity and strain hardening at relatively low draw ratios (e.g. $1 < \lambda < 10$)

Polymer	Thermal treatment	Strain hardening $(\partial\sigma/\partial\lambda)_{\dot{\epsilon}}$	Strain rate sensitivity $(\partial\sigma/\partial\dot{\epsilon})_{\lambda}$	λ_{peak}	$\dot{\epsilon}_{peak}$	$\dot{\epsilon}$–λ peak width
HGUR						
$\bar{M}_w \sim 3 \times 10^6$	–	High	High	Low	Low	Very narrow
H020	Slow cooled	Medium	Medium High	Medium	Low	Narrow
$\bar{M}_w \sim 3 \times 10^5$	Quenched	Medium	Medium Low	Medium	High	Very narrow
R50	Slow cooled	Low	High	High	Low	Very broad
$\bar{M}_w \sim 1 \times 10^5$	Quenched	Low	Low	High	High	Broad

also be determined by the polymer deformation behaviour. Consider the point at which $\dot{\epsilon} = \dot{\epsilon}_{peak}$ where

$$\frac{d\dot{\epsilon}}{d\lambda} = 0$$

i.e. $$\frac{d\sigma}{d\lambda} = \left(\frac{\partial\sigma}{\partial\lambda}\right)_{\dot{\epsilon}_{peak}}$$ from Equation 18

Now $$\frac{d\sigma}{d\lambda} = \frac{Lg}{A_0}$$ from Equation 5

so that

$$L = \frac{A_0}{g}\left(\frac{\partial\sigma}{\partial\lambda}\right)_{\dot{\epsilon}_{peak}} \quad (19)$$

The draw load is therefore fixed by the strain hardening at $\dot{\epsilon}_{peak}$, the strain rate sensitivity being involved in fixing the value of $\dot{\epsilon}_{peak}$ and hence $(\partial\sigma/\partial\lambda)_{\dot{\epsilon}_{peak}}$.

4.2.2. Supporting tensile drawing data

The strain hardening behaviour and strain rate sensitivity may really only be inferred from the observed neck profiles: in the neck σ, λ and $\dot{\epsilon}$ are changing simultaneously. However, support for the above interpretations can be obtained by careful experiments to collect true stress–strain–strain rate data, to allow observation of the strain hardening and strain rate dependence of the draw stress independently. Such work has already been published for slow cooled R50 LPE drawn at 100° C [4]. Further work, identical in nature to that described in [4] has now been performed, investigating the true σ–λ–$\dot{\epsilon}$ behaviour of R50S at 75° C and H020S at 100 and 75° C, and the results are presented in Figs. 11 and 12 in the form of true stress draw ratio curves at constant true strain rate. These curves clearly indicate that H020S strain hardens much more rapidly than R50S at the same draw temperature. However, the strain rate sensitivity is roughly the same for each material. These observations bear out qualitatively the interpretation of the neck profiles discussed above: H020S exhibits a more gentle geometrical neck profile and a lower λ_{max} than R50S (Fig. 3) due to a higher strain hardening.

Quantitative predictions of the neck profiles have been attempted, using empirical expressions for $(\partial\sigma/\partial\lambda)_{\dot{\epsilon}}$ and $(\partial\sigma/\partial\dot{\epsilon})_{\lambda}$, obtained from the tensile data. A typical prediction of the $\dot{\epsilon}$–λ curve is shown in Fig. 13 for H020S at 100° C. The agreement between the predicted curve and that obtained experimentally is satisfactory, considering the dependence of the prediction on σ–λ–$\dot{\epsilon}$ data for low draw ratios, where such data is very difficult to collect and hence not sufficiently plentiful. The calculation of strain rate increments from Equation 18 is very sensitive to the values of each of the terms, and the whole computation depends strongly on the starting point, namely a reliable value of neck profile velocity.

Consideration of Figs. 11 and 12 also suggests that the strain hardening (measured by $(\Delta\sigma/\Delta\lambda)_{\lambda,\dot{\epsilon}}$) does change approximately uniformly with draw temperature across the range of λ and $\dot{\epsilon}$ investigated, as was inferred from the slight change in neck profile with set draw temperatures, although these measurements clearly have considerably restricted accuracy.

It is unfortunately not possible to obtain true σ–λ–$\dot{\epsilon}$ data for quenched morphology specimens at low draw ratios, as discussed in [16]. It now appears that the true σ–λ–$\dot{\epsilon}$ behaviour for these materials may be inferred from the neck shape.

4.2.3. Non-isothermal and pressure effects

The deformation behaviour has previously been considered under isothermal conditions, at constant hydrostatic pressure, P, and for reasons detailed above we consider that this is justified. However, a fuller expression of the total differential $d\sigma$ is

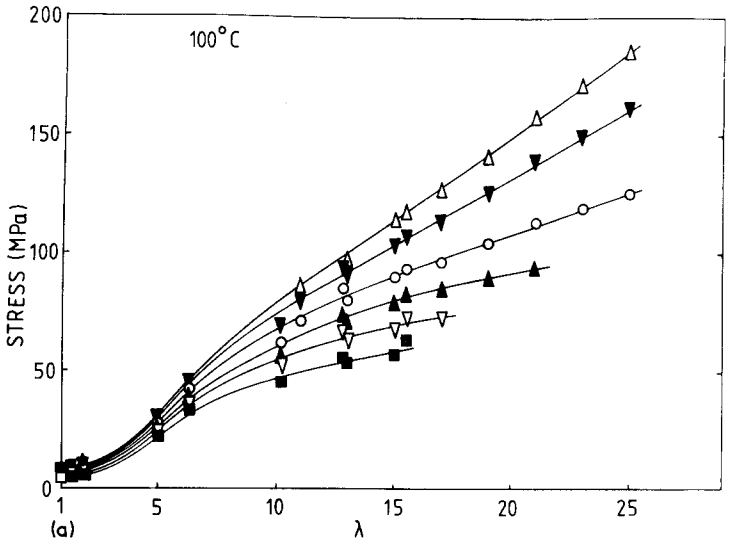

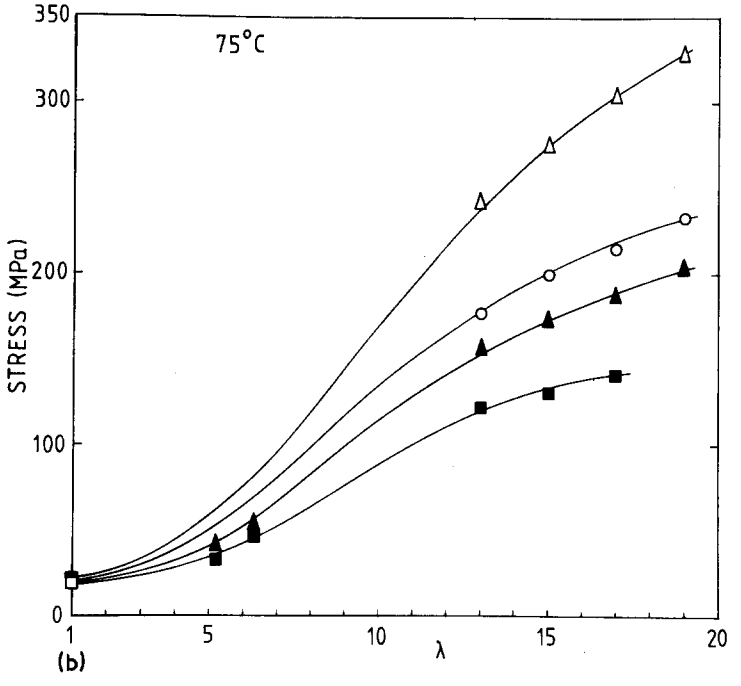

Figure 11 True stress–draw ratio curves at constant true strain rates for R50 S. (Strain rates (sec^{-1}) △, 5×10^{-2}; ▼, 2.5×10^{-2}; ○, 10^{-2}; ▲, 5×10^{-3}; ▽, 2.5×10^{-3}; ■, 10^{-3}; ●, 5×10^{-4}.)

$$d\sigma = \left(\frac{\partial\sigma}{\partial\lambda}\right)_{\dot{\epsilon},T,P} d\lambda + \left(\frac{\partial\sigma}{\partial\dot{\epsilon}}\right)_{\lambda,T,P} d\dot{\epsilon} + \left(\frac{\partial\sigma}{\partial T}\right)_{\lambda,\dot{\epsilon},P} dT + \left(\frac{\partial\sigma}{\partial P}\right)_{\lambda,\dot{\epsilon},T} dP \quad (20)$$

If we now consider $dP = 0$, but non isothermal drawing, then

$$d\dot{\epsilon} = \frac{\left[d\sigma - \left(\frac{\partial\sigma}{\partial\lambda}\right)_{\dot{\epsilon},T} d\lambda - \left(\frac{\partial\sigma}{\partial T}\right)_{\lambda,\dot{\epsilon}} dT\right]}{\left(\frac{\partial\sigma}{\partial\dot{\epsilon}}\right)_{\lambda,T}}. \quad (21)$$

Now $(\partial\sigma/\partial T)_{\lambda,\dot{\epsilon}}$ is negative (e.g. [4]), so an increase in temperature ($dT > 0$) will have the effect of *increasing* $d\dot{\epsilon}$. (Furthermore, the $(\partial\sigma/\partial\lambda)_{\dot{\epsilon},T}$ term will decrease, as will $(\partial\sigma/\partial\dot{\epsilon})_{\lambda,T}$ – both of which also increase $d\dot{\epsilon}$). Thus a temperature increase during drawing will have the effect of accentuating strain rates in the neck and possibly modifying the observed neck profile. It is difficult to predict exactly how this profile would be modified. For example, if the heat generated is greater at higher draw ratios, then the $\dot{\epsilon}$–λ peak may be broadened, and λ_{peak} shifted to the higher values. However the effects of heat

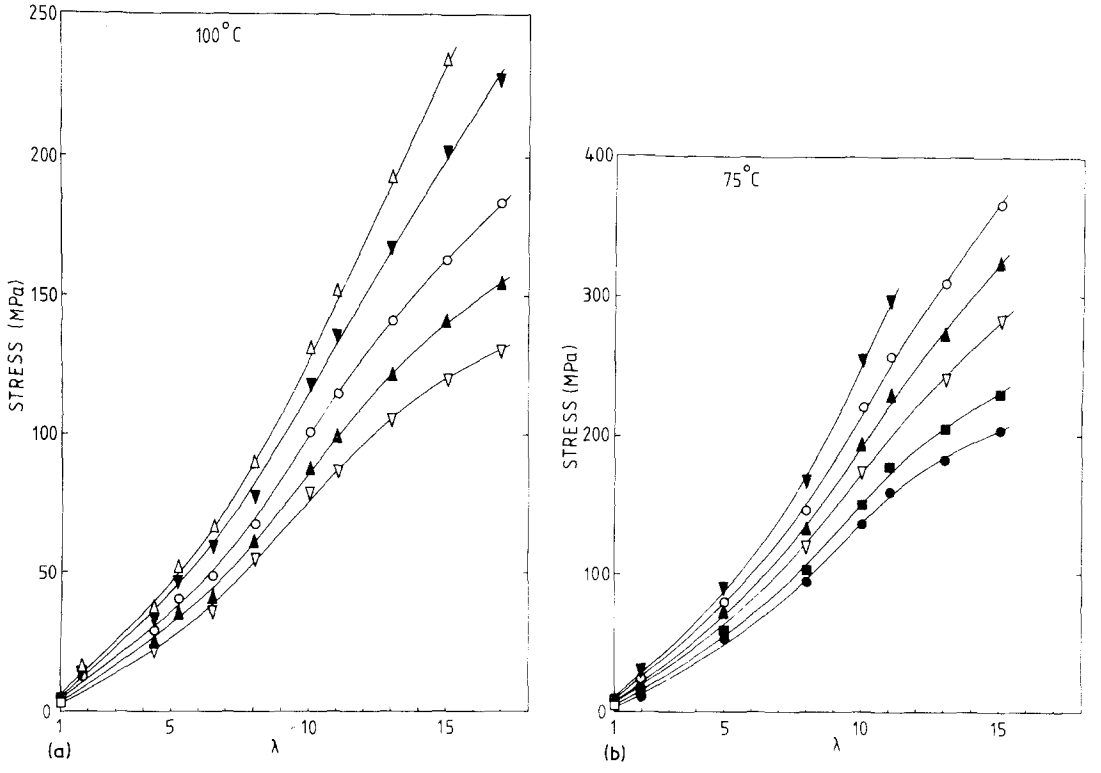

Figure 12 True stress–draw ratio curves at constant true strain rates for H020 S. (Strain rate symbols as for Fig. 11).

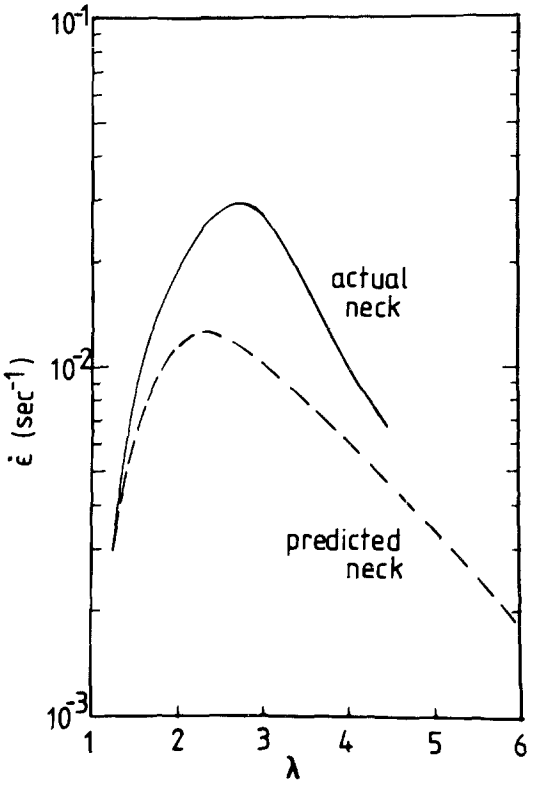

Figure 13 Predicted $\dot{\epsilon}$–λ curve for H020S, 100° C.

transfer may play a part – the higher λ material is thinner and has a higher axial thermal conductivity than lower λ material [21], both of which might lead to a more rapid transfer of heat from high λ material than from low λ material.

The effects of change in hydrostatic pressure, P, at constant temperature are opposite to those of change in temperature. The term $-(\partial\sigma/\partial P)_{\lambda,\dot{\epsilon}}dP$ would be introduced into the numerator of Equation 21. Now $(\partial\sigma/\partial P)_{\lambda,\dot{\epsilon}}$ is a positive quantity. Thus increases in pressure would lead to a decrease in $d\dot{\epsilon}$ at constant temperature, so modifying the neck profile observed. The tensile draw stress gives rise to a hydrostatic component of stress which has been ignored in the previous discussion – this component, will, of course, vary as $\sigma(x)$ varies through the neck.

5. Conclusions

1. A simple model of the neck, in which a constant neck profile (once formed) propagates into the isotropic material at a constant velocity, v_p, for a given LPE grade and fixed drawing conditions, has been found satisfactory for describing the behav-

iour of various LPE grades in uniaxial tension. The machine imposed boundary condition, i.e. the average axial strain rate in the neck, which is equal to the machine strain rate, has been used to predict values of v_p for each LPE grade which were found to be in reasonable agreement with experimental measurements.

2. The geometrical neck profile, steady draw ratio produced through the neck, and the steady draw load for each grade have *all* been related to the true stress–draw ratio–true strain rate surface at the relevant temperature, via the strain hardening behaviour and the strain rate sensitivity which are particular slopes of the true σ–λ–$\dot{\epsilon}$ surface. Thus, inside the overall boundary condition of an imposed extension rate which fixes the average axial strain rate, the strain hardening behaviour and strain rate sensitivity of the particular grade fix the observed neck geometry, the steady draw load and the maximum steady draw ratio produced through the neck. The neck shape for isothermal drawing therefore provides an indication of the nature of the true σ–λ–$\dot{\epsilon}$ surface for different grades, and hence possible advantages or limitations in predominantly tensile deformation operations on the solid polymer.

3. Support for this interpretation of the neck profile has been given, using tensile drawing data for two of the LPE grades, in the form of true stress–draw ratio curves at constant true strain rate, these curves being a two dimensional representation of the true σ–λ–$\dot{\epsilon}$ surface.

4. Related to the above findings, the molecular weight has been observed to have an influence on the strain hardening behaviour – in general the higher molecular weight grades exhibit a greater degree of strain hardening $(\partial\sigma/\partial\lambda)_{\dot{\epsilon},T,P}$, at a given draw ratio. The morphology of each specimen has also been observed to have an influence on the strain rate sensitivity, which is related to $(\partial\sigma/\partial\dot{\epsilon})_{\lambda,T,P}$, with slow cooled morphologies exhibiting a greater strain rate sensitivity than water quenched morphologies.

References

1. P. I. VINCENT, *Polymer* 1 (1960) 7.
2. *Idem*, "Physical Basis of Yield and Fracture", Institute of Physics Conference, Oxford (Institute of Physics, London, 1966) p. 155.
3. I. M. WARD, "Mechanical Properties of Solid Polymers" (John Wiley, London, 1971) p. 271.
4. P. D. COATES and I. M. WARD, *J. Mater. Sci.* 13 (1978) 1957.
5. N. J. MILLS, *Brit. Polymer J.* 10 (1978) 1.
6. A. S. ARGON, American Society for Metals Seminar on Inhomogeneity of Plastic Deformation, Detroit, 1971.
7. G. CAPACCIO and I. M. WARD, British Patent Applications 52644/74, 52647/74, 52654/74.
8. G. CAPACCIO, A. G. GIBSON and I. M. WARD in "Ultra High Modulus Polymers" edited by A. Cifferri and I. M. Ward, Ch. 1. (Applied Science Publishers, London, 1979).
9. D. L. M. CANSFIELD, G. CAPACCIO and I. M. WARD, *Polymer Eng. Sci.* 16 (1976) 721.
10. P. D. COATES and I. M. WARD, *Polymer* 20 (1979) 1553.
11. B. BREW and I. M. WARD, *ibid.* 19 (1978) 1337.
12. G. CAPACCIO, T. A. CROMPTON and I. M. WARD, *J. Polymer Sci., Polymer Phys. Ed.* 14 (1976) 1641.
13. G. CAPACCIO, I. M. WARD, M. A. WILDING and G. F. LONGMANN, *J. Macromol. Sci.* B15 (1978) 381.
14. P. D. COATES, A. G. GIBSON and I. M. WARD, *J. Mater. Sci.* 15 (1980) 359.
15. B. AVITZUR, "Metal Forming: Processes and Analysis", (McGraw Hill, New York, 1968).
16. R. HILL, "Mathematical Theory of Plasticity" (Clarendon Press, Oxford, 1950) pp. 272–7.
17. O. RICHMOND and M. L. DEVENPECK, Proceedings of the 4th US National Congress on Applied Mechanics, (1962) p. 1053.
18. M. L. DEVENPECK and O. RICHMOND, *J. Eng. Ind., Trans. ASME* B87, (1965) 425.
19. O. RICHMOND and H. L. MORRISON, *J. Mech. Phys. Solids* 15 (1967) 195.
20. R. T. SHIELD, *Proc. Roy. Soc. A* 233 (1955) 267.
21. A. G. GIBSON, D. GREIG, M. SAHOTA, I. M. WARD and C. L. CHOY, *J. Polymer Sci. Polymer Lett. Edn.* 15 (1977) 183.
22. J. H. MAYER, R. N. HAWARD and J. N. HAY, *J. Polymer Sci.* to be published.
23. C. BAUWENS-CROWET, *J. Mater. Sci.* 8 (1973) 968.

Received 17 September 1979 and accepted 25 April 1980.